frontiers | Frontiers in Physics

TYPE Original Research
PUBLISHED 14 September 2023
DOI 10.3389/fphy.2023.1240731

OPEN ACCESS

EDITED BY
Marco Sacchi,
University of Surrey, United Kingdom

REVIEWED BY
Yukun Lu,
China University of Petroleum, China
Jatis Kumar Dash,
SRM University, India

*CORRESPONDENCE
I. M. N. Groot,
✉ i.m.n.groot@lic.leidenuniv.nl

RECEIVED 15 June 2023
ACCEPTED 04 September 2023
PUBLISHED 14 September 2023

CITATION
Prabhu MK and Groot IMN (2023), From a Co-Mo precursor to 1H and 1T Co-promoted MoS_2: exploring the effects of gas pressure.
Front. Phys. 11:1240731.
doi: 10.3389/fphy.2023.1240731

From a Co-Mo precursor to 1H and 1T Co-promoted MoS_2: exploring the effects of gas pressure

M. K. Prabhu and I. M. N. Groot*

Leiden Institute of Chemistry, Leiden University, Leiden, Netherlands

The work presented in this paper makes use of the high-pressure *in situ* imaging capabilities of the ReactorSTM to demonstrate that single layer 1T Co-promoted MoS_2 can be directly synthesized without the use of any intercalating agents by applying highly reducing conditions during the growth. In this work, we have sulfided a CoMo nanoparticle precursor supported on Au(111) using a H_2:CH_3SH gas mixture at 1 bar and imaged the crystallization process *in situ* using the ReactorSTM. We have observed that at low temperatures (~500 K), an intermediate disordered $CoMoS_x$ phase is formed which crystallizes into metallic single-layer 1T Co-promoted MoS_2 slabs at temperatures close to 600 K. We also show that semiconducting 1H Co-promoted MoS_2 slabs synthesized under sulfur-rich conditions using a vacuum physical vapor deposition process, do not transform into their metallic 1T counterparts when exposed to the same reducing gas pressures and temperatures, thus, demonstrating the importance of the highly reducing conditions during the crystallization process for inducing the formation of the metastable 1T phase. XPS spectra of the 1T Co-promoted MoS_2 slabs indicate a sulfur deficiency of up to 11% in the top layer S, suggesting the likely role of sulfur vacancies in the formation of the 1T phase.

KEYWORDS

1T Co-promoted MoS_2, scanning tunneling microscopy, atmospheric-pressure studies, *in situ*, X-ray photoelectron spectroscopy

1 Introduction

Single-layer transition metal dichalcogenides (TMDCs) based on MoS_2 have garnered a lot of attention in both fundamental and applied research over the last several decades. A classic example of such an MoS_2-based TMDC is Co-promoted MoS_2 which is very important for many globally-relevant applications involving optoelectronics, heterogeneous catalysis, and electrocatalysis. For instance, catalysts based on Co-promoted MoS_2, a transition metal dichalcogenide formed by sulfiding mixed Co-Mo nanoparticles, are used for reducing global SO_x emissions via hydroprocessing in petroleum refineries [1], mixed alcohol synthesis [2], selective olefin hydrogenation [3], and selective mercaptan synthesis [4, 5]. Co-promoted MoS_2 is also widely used as a noble-metal-free electrocatalyst for the hydrogen evolution reaction (HER) [6] and Li-ion battery electrodes [7]. Particularly, its 1T metastable counterpart, has been of great relevance to van der Waals heterostructure-based optoelectronic devices due to its room temperature ferromagnetism [8–11].

In the laboratory, the 1T and 1T' analogues of pristine and promoted MoS_2 can be synthesized by various strategies. One of the techniques involves using alkali metals like Li, Na, or K during the MoS_2 synthesis. The alkali metals intercalate in the MoS_2 van der Waals gap and stabilize the 1T and 1T' phases, thus lowering the bandgap for the metastable phase formation with Mo in an octahedral coordination environment [12–17]. This technique has been used to synthesize and explore applications of Na- and K-doped single-layer MoS_2 and Co-promoted MoS_2 for gas-phase and HER catalysis [5, 18]. Intercalation with electron-donating aromatic amines has also proven to be successful in inducing the phase transformation from 1H to 1T [19]. An alternative synthesis strategy for the 1T or 1T' MoS_2 phase involves using a sulfur-deficient environment during the synthesis by lowering the chemical potential of sulfur [15, 20]. Additionally, using argon ion bombardment of 2H MoS_2 has been shown to generate local 1T mosaic structures [21]. The sulfur vacancy may also be generated by doping with a foreign metal atom of a different formal charge, for instance, Ru or substitutionally co-doping Ni and Co, to generate the 1T phase from the 2H phase [22, 23]. Similarly, oxygen doping has also been used as a technique to generate sulfur vacancies, and thereby, induce the formation of the 1T phase [24]. Electrochemical incorporation of S vacancies to induce a 2H–1T phase transition has also been reported [25]. Chalcogen vacancies in other Mo TMDCs have also been shown to induce a phase transition to the 1T and 1T' counterpart [26]. These experiments have generated a lot of excitement in the scientific community, because 1T polymorphs of MoS_2 have been shown to have high hydrogen evolution activity due to its metallic nature, unlike the 1H counterpart, and have been explored for applications in energy production and storage devices, in addition to applications in spintronics due to room temperature ferromagnetism [27–30]. Especially, many metastable 1T and 1T' phases of Co-doped MoS_2 have been demonstrated to be very competitive noble metal-free alternatives for green hydrogen production via water splitting, which has generated a lot of interest in the synthesis of 1T and 1T' counterparts of Co-promoted MoS_2 [6, 31, 32].

Based on these experimental findings, we hypothesize that it should be possible to directly synthesize 1T Co-promoted MoS_2 slabs from metallic Co and Mo nanoparticles by maintaining highly reducing environments during the synthesis, e.g., through a combination of hydrogen gas and the sulfiding agent. Use of hydrogen during the crystallization is expected to generate S-vacanies on the edges and the basal plane. According to the recent work of Jin et. al. [20], formation of edge S defects and edge sulfur saturations of less than 50% can kinetically favor the formation of the 1T phase by layer sliding. Additionally, the ease of hydrogen dissociation on under-coordinated and metallic Mo [33, 34] during the synthesis may even allow for some stabilization of the Co-promoted MoS_2 slabs through hydride intercalation. Based on the works of Mom et. al. and Grønborg et. al. [33, 34], such reducing conditions can be achieved by using background pressures of hydrogen approaching several bars, typically not possible in an ultra-high vacuum (UHV) setup. Furthermore, using a lower temperature for sulfidation may arrest the transition to the 2H phase. For instance, heating K-promoted MoS_2 to 650 K and above, under high gas pressures has been observed to induce irreversible transition to the 1H phase [5]. Burkhanov et. al. have shown that hydrogen intercalation achieved using H plasma under vacuum environments leads to lattice expansion of MoS_2 similar to that from the 1H to 1T phase transition [35].

In order to test our hypothesis, we have sulfided a precursor containing mixed Co-Mo nanoparticles supported on Au(111) under high-pressure sulfo-reductive conditions and observed *in situ* the crystallization process using the ReactorSTM setup. At temperatures of up to ~500 K, a disordered $CoMoS_x$ phase is observed to form which then crystallizes into single-layer 1T Co-promoted MoS_2 when the temperature is raised to 600 K. Sulfiding an identical CoMo precursor using H_2S under vacuum results in the formation of 1H Co-promoted MoS_2 slabs which do not transform into the 1T counterpart when exposed to the same sulfo-reductive conditions, suggesting that reducing conditions are necessary during the crystallization step to form the 1T phase. XPS spectra acquired post synthesis show that the 1T Co-promoted MoS_2 slabs are largely sulfur-deficient, suggesting the role of sulfur vacancies in metastable phase formation. Thus, we demonstrate that the 1T Co-promoted MoS_2 can be readily synthesized and stabilized by using a lower sulfidation temperature and sufficiently sulfo-reductive conditions, without the need for any additional intercalating agents. Furthermore, the ability to observe the formation of a metastable 1T Co-MoS_2 phase *in situ* (i.e., *while it happens*) with atomic resolution under 1 bar of gas pressure, elevated temperature, and aggressive chemical conditions, is the main novelty of this work, as it has remained an experimental challenge to do so for several decades. Additionally, the experimental observation that elevating the gas pressure to attain sufficiently reducing conditions to favor the formation of 1T Co-MoS_2 without the need of an intercalating agent is a very important finding that provides us a fundamental understanding of the 1T phase formation process and is also an additional novelty. To the best of our knowledge, the experimental work presented in this paper has not been carried out elsewhere in the past.

2 Materials and Methods

2.1 Sample cleaning

All the experiments were carried out in the ReactorSTM setup [36]. The sample cleaning procedure reported in our previous works has been used [37]. Briefly, a polished Au(111) crystal was cleaned by a cyclic sputtering and annealing procedure until XPS could no longer detect any impurities (<0.001 monolayers (ML)). 1.5 keV Ar^+ ions were used for the sputtering and annealing at 873 K was performed using radiative heating from a thoriated-tungsten filament at the back of the sample.

2.2 Physical vapor deposition (PVD)

To grow Mo and Co nanoparticles, Mo and Co rods of 99.99% purity purchased from Goodfellow were used. The evaporation of the respective metals was carried out using an EGCO4 e-beam evaporator. During the evaporation, the clean Au(111) sample was held at room temperature until the coverage of the respective metal was measured to be ~0.2 monolayers (ML). The coverage was

measured by analyzing the XPS spectra of Co and Mo with respect to Au(111) surface layers. Identical samples were prepared for the low-pressure and high-pressure sulfidation.

2.3 Low-pressure sulfidation

The mixed Co-Mo nanoparticles supported on Au(111) were sulfided at 650 K in a 2×10^{-6} mbar H_2S atmosphere. The heating from room temperature to 650 K was carried out in the same H_2S background at a rate of 4 K/s and held at 650 K for 20 min. The sample was then cooled in the H_2S background to 450 K over 15 min and thereafter, to room temperature in UHV over 150 min.

2.4 High-pressure sulfidation

The high-pressure sulfidation of the mixed Co-Mo precursor was carried out in the ReactorSTM. For this purpose, a sulfo-reductive gas mixture containing 9 H_2: 1 CH_3SH at a total pressure of 1 bar was chosen as the sulfiding agent. A temperature of 603 K was used for sulfidation as this is the highest temperature attainable in the ReactorSTM [38, 39]. A temperature of 520 K was also selected as an intermediate temperature to observe the effect of temperature.

After loading the sample for sulfidation into the reactor, the STM was first pressurized to 0.1 bar with the sulfo-reductive mixture and thereafter, the temperature was raised to 520 K with a heating rate of 2 K/min. A slow heating rate was chosen because rapid heating would cause rupturing of the fluor-elastomer seals used for isolating the ReactorSTM from the rest of the UHV. After this step, the total pressure was raised to 1 bar at a rate of 0.1 bar/min. The system was allowed to reach thermal steady-state for 90 min in order to minimize the thermal drift. The STM tip was brought into tunneling contact thereafter and the scanning was commenced. After scanning for ~70 min, the tip was retracted, the sample temperature was raised to 603 K at 3 K/min, and the system was allowed to thermally stabilize for 30 min before continuing the STM scanning.

2.5 Scanning tunneling microscopy

STM scanning was performed with the ReactorSTM using both the UHV mode and the high-pressure mode. STM tips were prepared by cutting polycrystalline Pt-Ir 90–10 wires purchased from Goodfellow without further processing. Constant-current scans were performed using LPM video-rate scanning electronics described in detail elsewhere [40, 41]. Home-developed Camera software and WSxM were used for STM image processing [42, 42]. Line-by-line background subtraction was used for the ease of viewing of the STM images. All UHV scans were carried out at room temperature.

For the high-pressure STM imaging, the sample was loaded into the STM assembly and a Kalrez seal was placed between the sample and the reactor. Thereafter, the bellows of the reactor were actuated to close the reactor and establish the closed volume for introducing the reaction gases. Gas bottles of Ar (N5.0), H_2 (N5.0), and CH_3SH (N2.8) {dimethylsulfide and dimethyldisulfide are the primary impurities} procured from Westfalen AG were used for all the experiments. The gas purity was confirmed using a mass spectrometer before use. The gas lines were flushed with Ar and baked out at 423 K for 12 h to remove any residual water and volatiles before commencing all experiments presented in this work.

For the post-sulfidation characterization, depressurizing the ReactorSTM to UHV conditions is necessary. For this purpose, the total pressure in the ReactorSTM was reduced to 0.1 bar and the model catalyst was allowed to cool down to 373 K under the flow of gases over 15 min. Thereafter, the gases were pumped away, the ReactorSTM was brought under UHV conditions, and the sample allowed to cool to room temperature over 60 min.

2.6 X-ray photoelectron spectroscopy

A commercial SPECS Phoibos system equipped with an XRM50 X-ray source set to the Al K-alpha line and coupled to a monochromator was used to excite the sample with a 54.6° incidence angle and with the X-rays generated using an acceleration voltage of 10 kV, 250 W. A HSA3500 hemispherical analyzer with a pass energy of 30 eV was used to acquire all the XPS spectra reported in this paper. All spectra were calibrated using the peak position of the Au 4f signal (84.0 eV) of the Au(111) substrate. For all the acquired data, 30 integrations were performed to have a sufficiently high signal-to-noise ratio. XPSPEAK41 software was used for the peak deconvolution. Relative sensitivity factors for surfaces were obtained from literature [43]. Shirley background subtraction was performed for all the spectra and a non-linear least squares fit method was used for convergence. The XPS spectra were fit using mixed Gaussian (65%) –Lorentzian (35%) (GL) curves. Asymmetric GL curves were used to fit the spectra of Co $2p_{3/2}$. For the Mo 3d and S 2p, paired GL peaks with a constrained area ratio of 3:2 and 1:2, respectively, were used to account for the spin-orbit splitting. For Co 2p, the fitting is performed for the Co $2p_{3/2}$ component. All the signature peak positions are based on previously reported literature work and are tabulated in Table 1 along with the references.

3 Results and discussion

We first prepare identical precursors containing Co-Mo mixed nanoparticles supported on a clean Au(111) substrate by sequential physical vapor deposition (PVD) of 0.2 monolayers (ML) Mo metal, followed by 0.2 ML Co metal at room temperature. The exact synthesis procedure is detailed in the Materials and Methods section and in the Supplementary Materials.

First, as a control experiment, one of the identical Co-Mo precursors was sulfided at 650 K under 2×10^{-6} mbar of H_2S and cooled to room temperature according to the recipe detailed in the Materials and Methods section, in order to replicate the vacuum synthesis recipe of single layer 1H Co-promoted MoS_2 slabs on Au(111) [48]. After this step, the sample was loaded into the ReactorSTM operated in the UHV mode. Figure 1 shows a large-scale STM image thus obtained. In Figure 1, we observe the formation of atomically-flat hexagonal slabs which are identified as single-layer 1H Co-promoted MoS_2 slabs. Under the sulfur-rich

TABLE 1 XPS binding energies for various components used for peak fitting.

Components	Binding energy (BE) (eV)	ΔBE[a] (eV)	References
1H MoS_2 Mo $3d_{5/2}$	229.2	3.15	[5, 27, 44, 45]
1T MoS_2 Mo $3d_{5/2}$	228.3	3.15	[5, 27, 44, 45]
S $2p_{3/2}$ (1T MoS_2)	161.8	1.16	[5, 27, 44, 45]
S $2p_{3/2}$ (2D CoS_2, 1H MoS_2)	162.7	1.16	[5, 27, 37, 44–46]
S 2s	226.9		[5, 27, 37, 44–46]
CoS_2 main Co $2p_{3/2}$	778.1		[27, 44, 47]
CoS_2 satellites Co $2p_{3/2}$	781.1, 783.1		[27, 44, 47]
Co-MoS_2 main Co $2p_{3/2}$	778.6		[27, 44, 47]
Co-MoS_2 satellite Co $2p_{3/2}$	781.6, 783.6		[27, 44, 47]

[a]ΔBE, is the energy difference between the spin-orbit splitting components. For example, ΔBE(3d) = BE, $3d_{5/2}$–BE, $3d_{3/2}$.

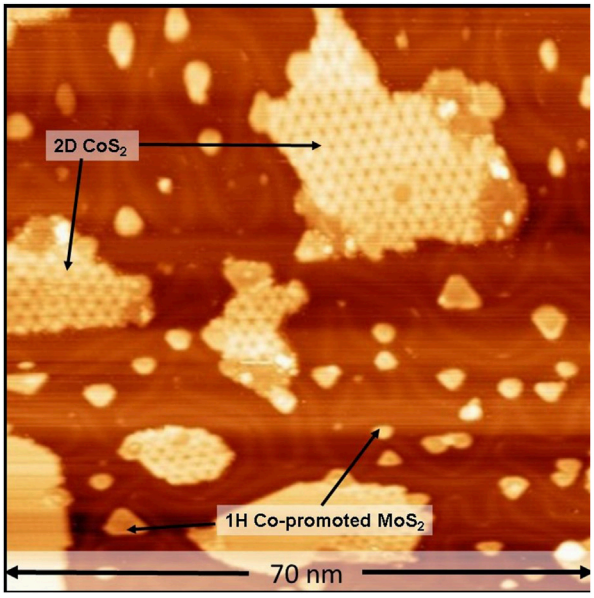

FIGURE 1
STM image of single-layer 1H Co-promoted MoS_2 slabs prepared by sulfidation of the Co-Mo precursor with H_2S (2×10^{-6} mbar). The STM image was acquired in UHV with a sample voltage of −1 V and tunneling current of 100 pA.

conditions used in this experiment, pristine MoS_2 slabs are known to display only the Mo-terminated edges due to the thermodynamic stability of the Mo-termination and hence, adopt a triangular shape [49]. The substitution of Mo atoms by Co along the S-terminated edges leads to the thermodynamic stability of the S-termination as well, thus, driving the formation of hexagon-shaped slabs such as those in Figure 1 [33]. The Co-promoted MoS_2 slabs have a bright outline along their periphery while their basal planes are imaged relatively darker. The darker basal plane is attributed to the semiconducting nature of 1H Co-promoted MoS_2 while the bright edge features are attributed to the 1D metallic edge states called BRIM sites [33]. Additionally, we also observe the formation of the single-layer 2D CoS_2 phase as a byproduct, with the characteristic hexagonal moiré structure which is 7 × 7 Au atoms (1.95 nm × 1.95 nm) wide. The 2D CoS_2 phase is also observed to form between the Co-promoted MoS_2 slabs on the Au(111) steps. These observations are in excellent agreement with our recent work on 2D CoS_2 slabs supported on Au(111) [46]. Furthermore, the observation of the complete conversion of the Co and Mo nanoparticles into the respective TMDC phases after the sulfidation process is in agreement with the prior experimental works on the sulfidation of Co and Mo nanoparticles under controlled vacuum conditions [33, 49, 50].

In order to test our hypothesis on the formation of 1T Co-promoted MoS_2 slabs under highly reducing conditions, a freshly prepared identical Co-Mo precursor was sulfided using high-pressure sulfo-reductive conditions within the ReactorSTM. For this purpose, a sulfo-reductive gas mixture (9:1 H_2:CH_3SH) was used to pressurize the ReactorSTM to 1 bar. Thereafter, the temperature was raised from room temperature to 520 K at a rate of 2 K/min. Figure 2A shows a large-scale STM image obtained *in situ* during the sulfidation under the sulfo-reductive gas mixture. We observed the formation of two phases: islands with a somewhat hexagonal shape and disordered arrangement of bright protrusions and large atomically-flat islands with an ordered hexagonal pattern, both of which are seen in Figures 2A, B.

The somewhat hexagon-shaped islands are identified as those of poorly crystalline molybdenum sulfide (MoS_x). Due to the presence of a sufficient number of diffusing cobalt atoms, we expect that any MoS_x phase formed will likely be doped with Co atoms, and hence, we denote this phase as $CoMoS_x$. The $CoMoS_x$ islands are measured to be 2.8 Å high (see heightline, Figure 2B), matching closely with the measured height of single-layer Co-promoted MoS_2 from previous experimental reports [33]. The $CoMoS_x$ islands are likely an intermediate phase towards the formation of crystalline Co-promoted MoS_2. No further changes are observed in this disordered $CoMoS_x$ phase up to 67 min into the scanning in the sulfo-reductive gas environment at 520 K (see Figures 2C, D), suggesting that the temperature is insufficient for any crystallization to occur.

The atomically-flat slabs with a hexagonal moiré pattern on their basal plane are identified as 2D CoS_2 islands. These slabs were also observed to form in our control experiment (see Figure 1).

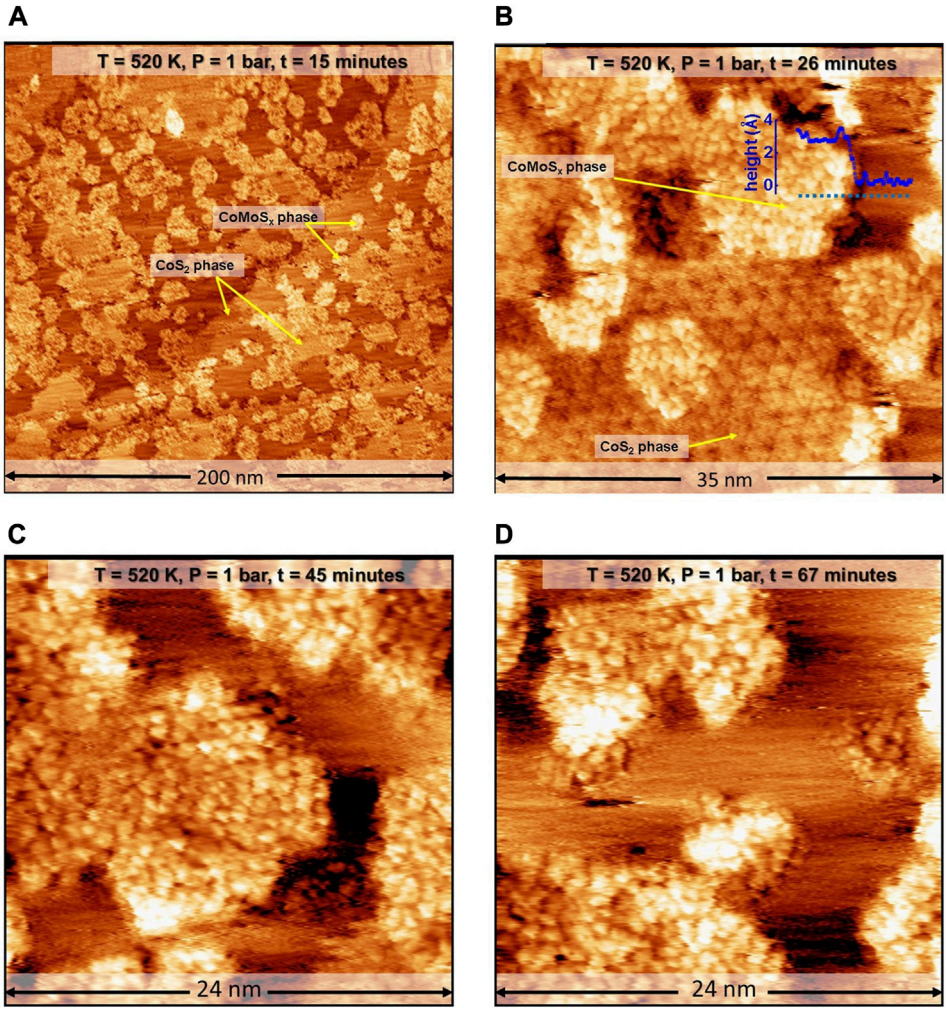

FIGURE 2
(A–D) STM images of the Co-Mo precursor acquired *in situ* during the sulfidation by a sulfo-reductive gas mixture (1 bar, $9H_2$: $1CH_3SH$) at 520 K. The MoS_x and 2D CoS_2 phases are identified. The STM images were aquired at −0.3 V sample voltage and 500 pA tunneling current. The "t" indicated in the label bars at the top of each STM image indicates the time stamp of acquisition from the commencing of the scanning.

The 2D CoS_2 also retains the characteristic hexagonal moiré structure indicating that the basal plane of 2D CoS_2 does not undergo significant structural changes under the sulfo-reductive gas mixture used. Additionally, the formation of this moiré structure shows that the 2D CoS_2 islands are crystalline in nature and that the sulfidation of Co nanoparticles is already complete during the process of bringing the ReactorSTM to the operating conditions. This rapid spread and reaction of Co is attributed to the cluster diffusion behavior of Co nanoparticles in the presence of S adatoms which leads to rapid growth of 2D CoS_2 [50].

To speed up the process of $CoMoS_x$ crystallization, we further increased the temperature to 603 K at the rate of 2 K/min while maintaining the sulfo-reductive reaction gases and thermally stabilize the STM before commencing the scanning *in situ*. Figure 3A shows a large-scale STM image obtained *in situ* at 603 K at t = 121 min. Ten minutesafter attaining 603K, the edges of the $CoMoS_x$ islands are observed to appear slightly brighter in the STM images, as can be seen in Figure 3B. Over the next 35 min, the $CoMoS_x$ slabs are observed to crystallize from the step edges towards the interior (see Figures 3B–F). The crystallization is evident from the formation of an ordered hexagonal lattice. The new crystalline phase has a hexagonal arrangement of bright protrusions which are 0.33 ± 0.01 nm apart (see Figure 3F; height profile in Figure 3G). This matches closely with the basal plane S-S distance of single-layer MoS_2 and Co-promoted MoS_2 [49]. Furthermore, the basal plane protrusions are imaged bright with respect to gold, unlike the 1H Co-promoted MoS_2 in Figure 1, suggesting that this phase has a metallic nature. The crystalline Co-promoted MoS_2 formed under sulfo-reductive conditions (see Figures 3B–D), however, does not have a bright BRIM along the edges, unlike the 1H Co-promoted MoS_2 slabs in the control experiment (see Figure 1). All characteristics of this new crystalline phase formed in the sulfo-reductive environment agree very well with those reported for a metastable 1T-MoS_2 phase in which Mo is in an octahedral coordination environment [15, 28]. Therefore, we identify this new phase as that of single-layer 1T Co-promoted MoS_2. Figures 3B–D also show that the crystalline phase is not resolved well along

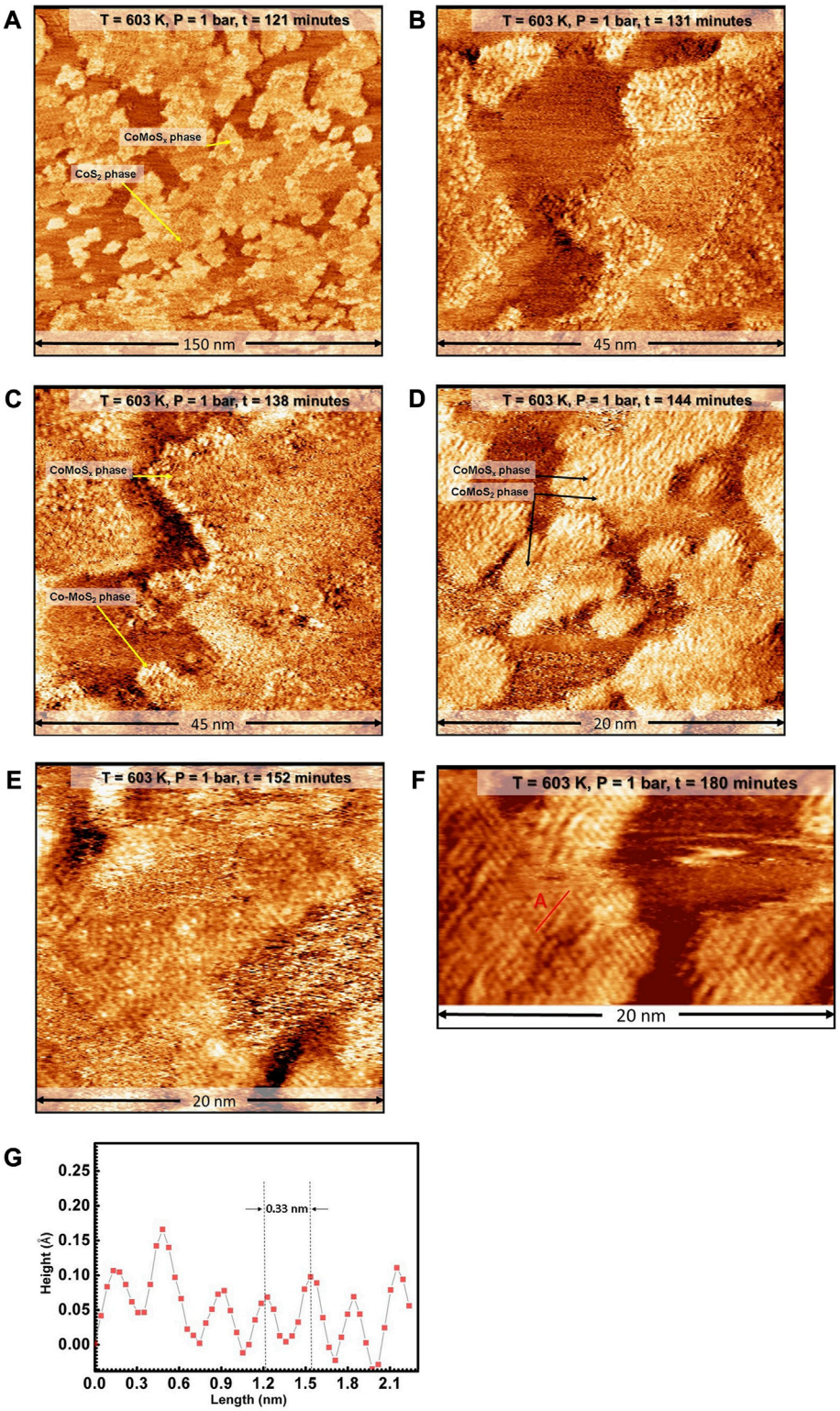

FIGURE 3
(A–F) STM images of the Co-Mo precursor acquired *in situ* during the sulfidation by a sulfo-reductive gas mixture (1 bar, $9H_2$: $1CH_3SH$) at 603 K. The MoS_x and 2D CoS_2 phases are identified. The STM images were aquired at −0.3 V sample voltage and 500 pA tunneling current. The "t" indicated in the label bars at the top of each STM image indicates the time stamp of acquisition from the commencing of the scanning. **(G)** Height profile along the red line marked A in F. E anf F have additional derivative enhancing in order to bring forward the detail for the ease of viewing.

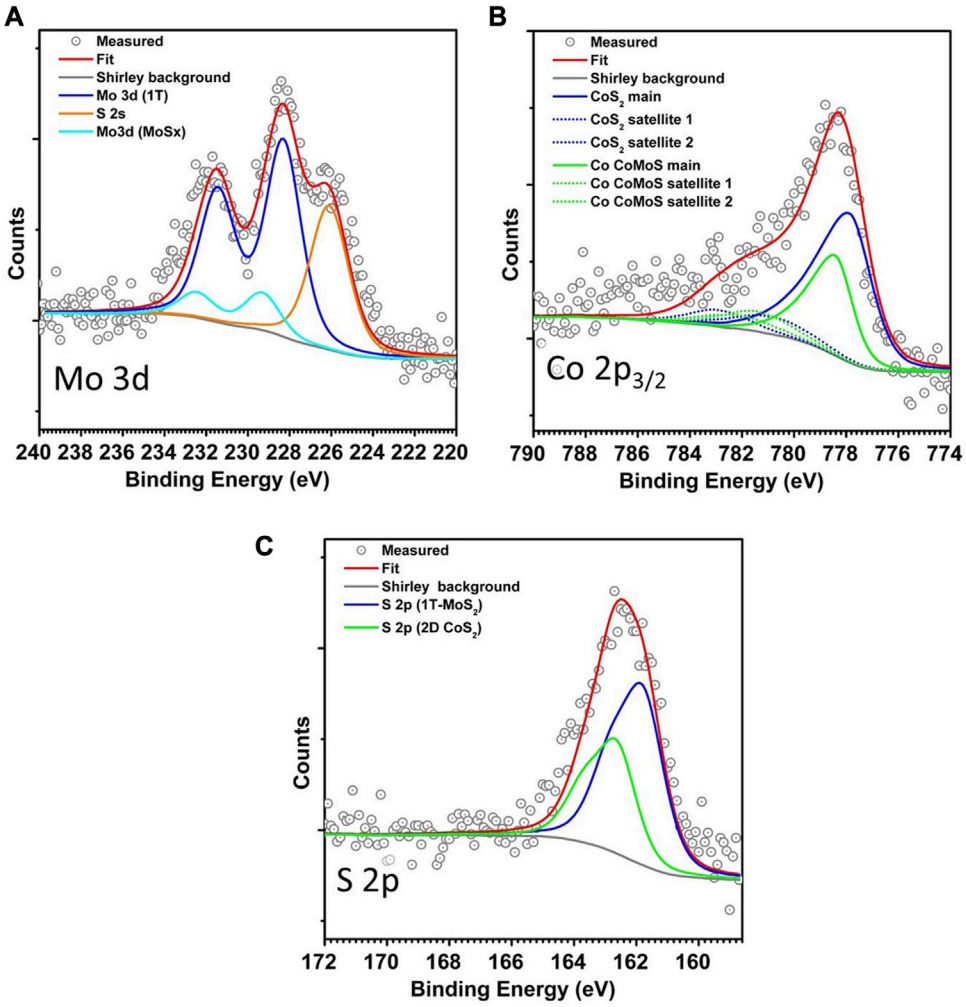

FIGURE 4
(A–C) Mo 3d, Co $2p_{3/2}$, and S 2p XPS spectra of the Co-Mo precursor supported on Au(111) after sulfidation in the high-pressure sulfo-reductive gases at 603 K.

one of the crystallographic directions especially along the slow scan direction (top to down), giving the appearance of lines. We attribute this to tip assymetry arising from interaction with the gases, especially CH_3SH at the elevated temperature and pressure used. Such effects were also observed by Mom et. al. under similar gas conditions when using similar as-cut Pt-Ir tips [34].

One may expect that employing a high partial pressure of hydrogen during the cyrstallization favors the formation of a large number of sulfur vacancies along the Co-MoS_2 edges and the basal plane. Recent theoretical work [20] has shown that increasing the number of sulfur vacancies can make translational layer sliding to form the 1T configuration more kinetically favorable in pristine MoS_2 slabs. While it may also be argued that the electron donation from Co also aids in the formation of 1T Co-promoted MoS_2, merely having the Co alone does not yield the formation of the 1T phase under the vacuum sulfidation-based control experiment. We also consider the possibility that using a different sulfiding agent may also aid in the formation of the 1T phase as we have used H_2S for our control experiment and CH_3SH for the high-pressure sulfidation as the sulfiding agents. Research carried out in the past has shown that the effect of sulfiding agents on the chemical potential of sulfur is minor for small thiol-containing molecules like H_2S and CH_3SH, as they all readily disssociate on the gold surface and form adsorbed–SH while aromatic (such as thiophenes) and doubly substituted thiols (like dimethyl sulfide) lead to a lower chemical potential of sulfur [33], [51–53]. Additionally, previous experiments using a variety of H_2:H_2S mixtures under vacuum pressures for MoS_2 synthesis did not lead to the formation of the 1T phase [49]. Therefore, the elevated H_2 gas pressure used in our experiment to form a sufficient number of sulfur vacancies remains as a major factor that assists in the formation of 1T Co-promoted MoS_2.

We make use of XPS analysis to determine the number of sulfur vacancies and the amount of Co incorporation into the edges of 1T Co-promoted MoS_2. As the 1T phase is metallic, BRIM sites are not present on the edges, making the identification of the Co-substituted S edges from the STM images alone difficult. XPS, on the other hand, can detect and resolve Co present in 1T MoS_2 and CoS_2 phases, albeit in a statistically averaged manner [9, 54]. Typically, the Co

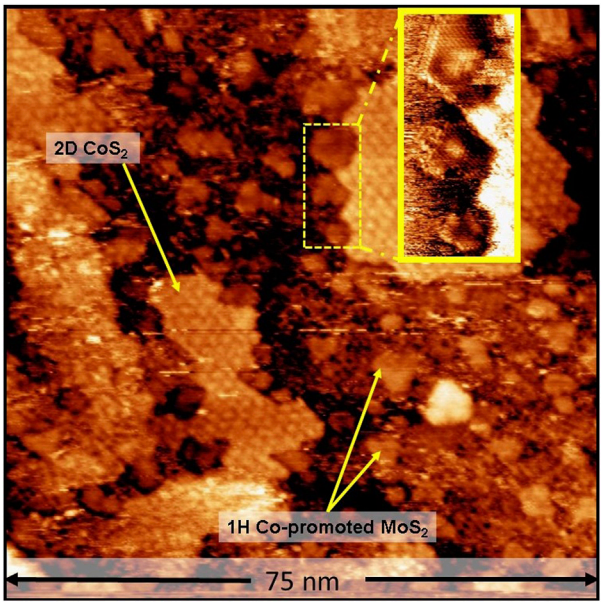

FIGURE 5
In situ STM image of vacuum-synthesized Co-promoted MoS_2 slabs after 6 h under the sulfo-reductive gas environment (1 bar, 9:1 H_2:CH_3SH, 603 K). The inset shows atom-resolved 1H Co-promoted MoS_2 slabs with BRIM sites. STM image acquired with a sample voltage of −0.3 V and tunneling current of 500 pA.

present on the S edges of 1H and 1T MoS_2 has a signal resembling metallic Co sulfide but shifted by 0.6–0.8 eV to higher binding energy depending on the metallicity of the support [9, 54, 55]. Additionally, the structural relaxation upon the transformation of the 1T phase into the 2H phase results in a downshift in binding energy of the Mo 3days and S 2p spectra of the 1T phase by ~0.9 eV with respect to the 1H phase, thus allowing for the identification of the 1T phase [56, 57]. Before measuring the XPS spectra, the sample exposed to high pressure was cooled to room temperature in the sulfo-reductive gas environment and then pumped down to UHV. Thereafter, XPS spectra of Mo 3d, S 2p and Co 2p were acquired and analyzed. The Mo 3d spectrum (see Figure 4A) shows the main Mo $3d_{5/2}$ peak at 282.3 eV which matches well with the reported XPS spectra of 1T-MoS_2 and 1T-Co-promoted MoS_2 [54, 57]. The component at 290.2 eV is attributed to the unconverted MoS_x phase as we did not observe any 1H Co-promoted MoS_2 in the STM images. The Co $2p_{3/2}$ spectrum (see Figure 4B) shows the presence of 2 types of cobalt species, namely, the Co in metallic 2D CoS_2 at 778.1 eV (55%) and the Co present on the edges of MoS_2 at 778.7 eV (45%). The corresponding S 2p spectrum (see Figure 4C) shows an asymmetric peak that consists of contributions from S in 2D CoS_2 and the 1T phase. Furthermore, comparing the overall signals of Co, Mo, and S, the molecuar formula of 1T Co-MoS_2 is determined to be $Mo_{0.67}Co_{0.32}S_{1.89}$, with 11% sulfur vacancies in the top layer (see Supplementary Material S1.2, Supplementary Table S2). The high number of sulfur vacancies is expected due to the highly reducing environment used during the synthesis in the ReactorSTM. In comparison, the molecular formula of the 1H Co-promoted MoS_2 from the control experiment is determined to be $Mo_{0.65}Co_{0.35}S_{2.05}$.

As an additional control experiment, the control sample containing 1H Co-promoted MoS_2 slabs grown using 2 × 10^{-6} mbar H_2S was loaded into the ReactorSTM and exposed to the high-pressure sulfo-reductive gas mixture (9:1 H_2:CH_3SH, 1 bar) at 603 K for up to 6 h. Figure 5 shows a large-scale STM image obtained *in situ* after 6 h. Comparing Figures 1, 5, we observe that the morphology of the Co-promoted MoS_2 slabs is largely preserved. Under these gas conditions, we expect that the edges of the Co-promoted MoS_2 slabs are reduced to the same degree as in our high-pressure sullfidation experiment since the gas conditions are identical. In Figure 5, we clearly observe that all the Co-promoted MoS_2 slabs remain in the 1H state and do not transform into the 1T state, as can also be seen in the atom-resolved inset where 1H Co-promoted MoS_2 slabs with BRIM sites

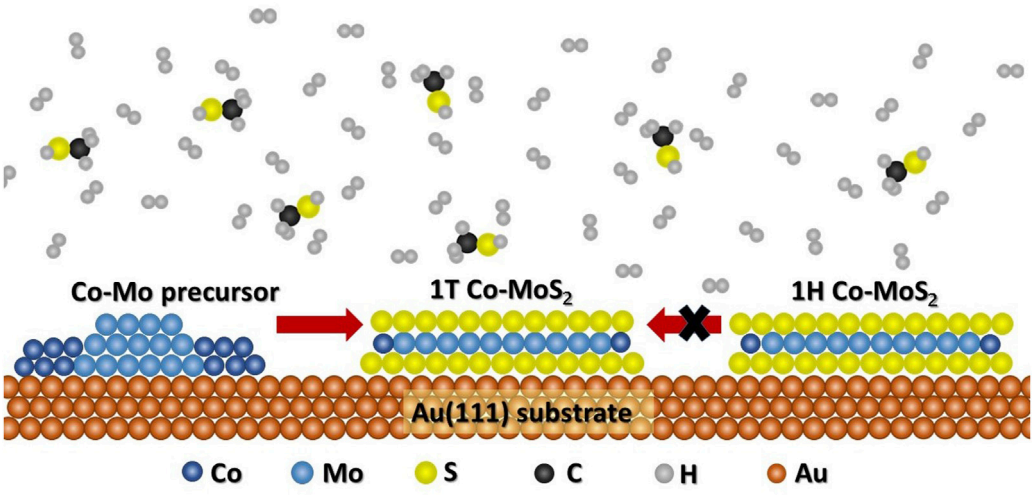

FIGURE 6
Schematic diagram describing the kinetically favorable and unfavorable routes for the 1T Co-promoted MoS_2 formation.

are clearly imaged. This shows that the 1T state is accessible at the gas conditions and temperatures used, if and only if, the thermodynamically stable 1H state has not already been formed. A schematic summarizing all our findings is shown in Figure 6.

4 Conclusion

We have demonstrated using the *in situ* STM imaging capabilities of the ReactorSTM, that using sufficiently reducing environments during the crystallization phase can favor the formation of metallic 1T Co-promoted MoS_2. On the other hand, if 1H Co-promoted MoS_2 is already formed, then there are large kinetic barriers that hinder the formation of a sufficient number of S vacancies to drive the transformation to the 1T phase through atomic S-layer sliding. These observations with the STM are confirmed and supported very well by the corresponding XPS spectra which show that the 1T Co-MoS_2 slabs have a large number of sulfur vacancies in comparison to the 1H Co-MoS_2 slabs. The formation of pure 1T Co-promoted MoS_2 under sulfo-reductive conditions without an alkali metal intercalator is remarkable as it demonstrates the feasibility for directly synthesizing monolayers of pure 1T or 1H Co-promoted MoS_2. This is of great relevance for fundamental research in optoelectronics, green hydrogen production, and heterogeneous and electro-catalysis.

Data availability statement

The original contributions presented in the study are included in the article/Supplementary Material, further inquiries can be directed to the corresponding author.

Author contributions

MP performed all experiments and analyzed all data. IG conceived and supervised the project. All authors contributed to the article and approved the submitted version.

Funding

This project received funding from the Leiden Institute of Chemistry, Leiden University.

Conflict of interest

The authors declare that the research was conducted in the absence of any commercial or financial relationships that could be construed as a potential conflict of interest.

Publisher's note

Supplementary material

The Supplementary Material for this article can be found online at: https://www.frontiersin.org/articles/10.3389/fphy.2023.1240731/full#supplementary-material

References

1. Sanders AFH, De Jong AM, De Beer VHJ, Van Veen JAR, Niemantsverdriet JW. Formation of cobalt-molybdenum sulfides in hydrotreating catalysts: A surface science approach. *Appl Surf Sci* (1999) 144–145:380–4. doi:10.1016/S0169-4332(98)00831-9

2. Taborga Claure M, Chai SH, Dai S, Unocic KA, Alamgir FM, Agrawal PK, et al. Tuning of higher alcohol selectivity and productivity in CO hydrogenation reactions over K/MoS_2 domains supported on mesoporous activated carbon and mixed MgAl oxide. *J Catal* (2015) 324:88–97. doi:10.1016/j.jcat.2015.01.015

3. Liu B, Liu L, Chai YM, Zhao JC, Liu CG. Essential role of promoter Co on the MoS_2 catalyst in selective hydrodesulfurization of FCC gasoline. *Ranliao Huaxue Xuebao/journal Fuel Chem Technol* (2018) 46(4):441–50. doi:10.1016/s1872-5813(18)30019-7

4. Gutiérrez OY, Kaufmann C, Hrabar A, Zhu Y, Lercher JA. Synthesis of methyl mercaptan from carbonyl sulfide over sulfide K $_2MoO_4/SiO_2$. *J Catal* (2011) 280(2): 264–73. doi:10.1016/j.jcat.2011.03.027

5. Yu M, Kosinov N, Van Haandel L, Kooyman PJ, Hensen EJM. Investigation of the active phase in K-promoted MoS_2 catalysts for methanethiol synthesis. *ACS Catal* (2020) 10(3):1838–46. doi:10.1021/acscatal.9b03178

6. Dai X, Du K, Li Z, Liu M, Ma Y, Sun H, et al. Co-doped MoS_2 nanosheets with the dominant CoMoS phase coated on carbon as an excellent electrocatalyst for hydrogen evolution. *ACS Appl Mater Inter* (2015) 7(49):27242–53. doi:10.1021/acsami.5b08420

7. Chen B, Liu E, He F, Shi C, He C, Li J, et al. 2D sandwich-like carbon-coated ultrathin TiO_2@defect-rich MoS_2 hybrid nanosheets: Synergistic-Effect-Promoted electrochemical performance for lithium ion batteries. *Nano Energy* (2016) 26: 541–9. doi:10.1016/j.nanoen.2016.06.003

8. Wang Y, Li S, Yi J. Electronic and magnetic properties of Co doped MoS_2 monolayer. *Sci Rep* (2016) 6:24153. doi:10.1038/srep24153

9. Nethravathi C, Prabhu J, Lakshmipriya S, Rajamathi M. Magnetic Co-doped MoS_2 nanosheets for efficient catalysis of nitroarene reduction. *ACS Omega* (2017) 2:5891–7. doi:10.1021/acsomega.7b00848

10. Sanikop R, Gautam S, Chae KH, Sudakar C. Robust ferromagnetism in Mn and Co doped 2D-MoS_2 nanosheets: Dopant and phase segregation effects. *J Magn Magn Mater* (2021) 2021:168226. doi:10.1016/j.jmmm.2021.168226

11. Lin X, Ni J. Charge and magnetic states of Mn-Fe-and Co-doped monolayer MoS 2. *J Appl Phys* (2014) 116(4). doi:10.1063/1.4891495

12. Silambarasan K, Archana J, Harish S, Navaneethan M, Sankar Ganesh R, Ponnusamy S, et al. One-step fabrication of ultrathin layered 1T@2H phase MoS_2 with high catalytic activity based counter electrode for photovoltaic devices. *J Mater Sci Technol* (2020) 51:94–101. doi:10.1016/j.jmst.2020.01.024

13. Liu L, Wu J, Wu L, Ye M, Liu X, Wang Q, et al. Phase-selective synthesis of 1T′ MoS $_2$ monolayers and heterophase bilayers. *Nat Mater* (2018) 17(12):1108–14. doi:10.1038/s41563-018-0187-1

14. Sharma CH, Surendran AP, Varma SS, Thalakulam M. 2D superconductivity and vortex dynamics in 1T-MoS_2. *Commun Phys* (2018) 1(1):90. doi:10.1038/s42005-018-0091-7

15. Xu H, Han D, Bao Y, Cheng F, Ding Z, Tan SJR, et al. Observation of gap opening in 1T′ phase MoS_2 nanocrystals. *Nano Lett* (2018) 18(8):5085–90. doi:10.1021/acs.nanolett.8b01953

16. Friedman AL, Hanbicki AT, Perkins FK, Jernigan GG, Culbertson JC, Campbell PM. Evidence for chemical vapor induced 2H to 1T phase transition in MoX_2 (X = Se, S) transition metal dichalcogenide films. *Sci Rep* (2017) 7(1):3836. doi:10.1038/s41598-017-04224-4

17. Rajapakse M, Karki B, Abu UO, Pishgar S, Musa MRK, Riyadh SMS, et al. Intercalation as a versatile tool for fabrication, property tuning, and phase transitions in 2D materials. *npj 2D Mater Appl* (2021) 5:30. doi:10.1038/s41699-021-00211-6

18. Palencia-Ruiz S, Uzio D, Legens C, Laurenti D, Afanasiev P. Stability and catalytic properties of 1T-MoS_2 obtained via solvothermal synthesis. *Appl Catal A Gen* (2021) 2021:118355. doi:10.1016/j.apcata.2021.118355

19. Kwon IS, Kwak IH, Abbas HG, Jung G, Lee Y, Park J, et al. Intercalation of aromatic amine for the 2H-1T′ phase transition of MoS_2 by experiments and calculations. *Nanoscale* (2018) 10(24):11349–56. doi:10.1039/c8nr02365d

20. Jin Q, Liu N, Chen B, Mei D. Mechanisms of semiconducting 2H to metallic 1T phase transition in two-dimensional MoS_2 nanosheets. *J Phys Chem C* (2018) 122(49): 28215–24. doi:10.1021/acs.jpcc.8b10256

21. Zhu J, Wang Z, Yu H, Li N, Zhang J, Meng J, et al. Argon plasma induced phase transition in monolayer MoS2. *J Am Chem Soc* (2017) 139(30):10216–9. doi:10.1021/jacs.7b05765

22. Zhang J, Xu X, Yang L, Cheng D, Cao D. Single-atom Ru doping induced phase transition of MoS_2 and S vacancy for hydrogen evolution reaction. *Small Methods* (2019) 3(12). doi:10.1002/smtd.201900653

23. Gao B, Zhao Y, Du X, Li D, Ding S, Li Y, et al. Electron injection induced phase transition of 2H to 1T MoS_2 by cobalt and nickel substitutional doping. *Chem Eng J* (2021) 2021:128567. doi:10.1016/j.cej.2021.128567

24. Ge J, Zhang D, Jin J, Han X, Wang Y, Zhang F, et al. Oxygen atoms substituting sulfur atoms of MoS_2 to activate the basal plane and induce the phase transition for boosting hydrogen evolution. *Mater Today Energ* (2021) 2021:100854. doi:10.1016/j.mtener.2021.100854

25. Gan X, Lee LYS, Wong KY, Lo TW, Ho KH, Lei DY, et al. 2H/1T phase transition of multilayer MoS_2 by electrochemical incorporation of S vacancies. *ACS Appl Energ Mater.* (2018) 1(9):4754–65. doi:10.1021/acsaem.8b00875

26. Hwang DY, Choi KH, Suh DH. A vacancy-driven phase transition in MoX_2 (X: S, Se and Te) nanoscrolls. *Nanoscale* (2018) 10(17):7918–26. doi:10.1039/c7nr08634b

27. Bremmer GM, Van Haandel L, Hensen EJM, Frenken JWM, Kooyman PJ. Instability of $NiMoS_2$ and $CoMoS_2$ hydrodesulfurization catalysts at ambient conditions: A quasi *in situ* high-resolution transmission electron microscopy and X-ray photoelectron spectroscopy study. *J Phys Chem C* (2016) 120(34):19204–11. doi:10.1021/acs.jpcc.6b06030

28. Shi S, Sun Z, Hu YH. Stabilization and applications of 2-dimensional 1T metallic MoS_2. *J Mater Chem A* (2018) 6:23932–77. doi:10.1039/c8ta08152b

29. Han SW, Park Y, Hwang YH, Jekal S, Kang M, Lee WG, et al. Electron beam-formed ferromagnetic defects on MoS_2 surface along 1 T phase transition. *Sci Rep* (2016) 6:38730. doi:10.1038/srep38730

30. Sanikop R, Budumuru AK, Gautam S, Chae KH, Sudakar C. Robust ferromagnetism in Li-intercalated and -deintercalated MoS_2 nanosheets: Implications for 2D spintronics. *ACS Appl Nano Mater* (2020) 3(12):11825–37. doi:10.1021/acsanm.0c02349

31. Ma F, Liang Y, Zhou P, Tong F, Wang Z, Wang P, et al. One-step synthesis of Co-doped 1T-MoS_2 nanosheets with efficient and stable HER activity in alkaline solutions. *Mater Chem Phys* (2020) 244:122642. doi:10.1016/j.matchemphys.2020.122642

32. Li P, Yang Y, Gong S, Lv F, Wang W, Li Y, et al. Co-doped 1T-MoS_2 nanosheets embedded in N, S-doped carbon nanobowls for high-rate and ultra-stable sodium-ion batteries. *Nano Res* (2019) 12(9):2218–23. doi:10.1007/s12274-018-2250-2

33. Grønborg SS, Salazar N, Bruix A, Rodríguez-Fernández J, Thomsen SD, Hammer B, et al. Visualizing hydrogen-induced reshaping and edge activation in MoS_2 and Co-promoted MoS2 catalyst clusters. *Nat Commun* (2018) 9(1):2211–11. doi:10.1038/s41467-018-04615-9

34. Mom RV, Louwen JN, Frenken JWM, Groot IMN. *In situ* observations of an active MoS_2 model hydrodesulfurization catalyst. *Nat Commun* (2019) 10(1):2546. doi:10.1038/s41467-019-10526-0

35. Burkhanov GS, Lachenkov SA, Kononov MA, Vlasenko VA, Mikhaylova AB, Korenovsky NL. Hydrogen intercalation of compounds with FeSe and MoS_2 layered crystal structures. *Inorg Mater Appl Res* (2017) 8:759–62. doi:10.1134/S2075113317050082

36. Herbschleb CT, Van Der Tuijn PC, Roobol SB, Navarro V, Bakker JW, Liu Q, et al. The ReactorSTM: Atomically resolved scanning tunneling microscopy under high-pressure, high-temperature catalytic reaction conditions. *Rev Sci Instrum* (2014) 85(8): 083703. doi:10.1063/1.4891811

37. Prabhu MK, Groot IMN. Simultaneous sulfidation of Mo and Co oxides supported on Au(111). *Phys Chem Chem Phys* (2021) 23(14):8403–12. doi:10.1039/d0cp03481a

38. Shafiq I, Shafique S, Akhter P, Yang W, Hussain M. Recent developments in alumina supported hydrodesulfurization catalysts for the production of sulfur-free refinery products: A technical review. *Catal Rev - Sci Eng* (2022) 64(1):1–86. doi:10.1080/01614940.2020.1780824

39. Brunet S, Mey D, Pérot G, Bouchy C, Diehl F. On the hydrodesulfurization of FCC gasoline: A review. *Appl Catal A: Gen* (2005) 278:143–72. doi:10.1016/j.apcata.2004.10.012

40. Rost MJ, Crama L, Schakel P, Van Tol E, Van Velzen-Williams GBEM, Overgauw CF, et al. Scanning probe microscopes go video rate and beyond. *Rev Sci Instrum* (2005) 76(5):053710. doi:10.1063/1.1915288

41. Rost MJ, van Baarle GJC, Katan AJ, van Spengen WM, Schakel P, van Loo WA, et al. Video-rate scanning probe control challenges: Setting the stage for a microscopy revolution. *Asian J Control* (2009) 11(2):110–29. doi:10.1002/asjc.88

42. Horcas I, Fernández R, Gómez-Rodríguez JM, Colchero J, Gómez-Herrero J, Baro AMWSXM. Wsxm: A software for scanning probe microscopy and a tool for nanotechnology. *Rev Sci Instrum* (2007) 78(1):013705. doi:10.1063/1.2432410

43. Wagner CD. Sensitivity factors for XPS analysis of surface atoms. *J Electron Spectros Relat Phenomena* (1983) 32(2):99–102. doi:10.1016/0368-2048(83)85087-7

44. Bremmer GM, van Haandel L, Hensen EJM, Frenken JWM, Kooyman PJ. The effect of oxidation and resulfidation on (Ni/Co)MoS_2 hydrodesulfurisation catalysts. *Appl Catal B Environ* (2019) 243:145–50. doi:10.1016/j.apcatb.2018.10.014

45. Cordova A, Blanchard P, Lancelot C, Frémy G, Lamonier C. Probing the nature of the active phase of molybdenum-supported catalysts for the direct synthesis of methylmercaptan from syngas and H_2S. *ACS Catal* (2015) 5(5):2966–81. doi:10.1021/cs502031f

46. Prabhu MK, Boden D, Rost MJ, Meyer J, Groot IMN. Structural characterization of a novel two-dimensional material: Cobalt sulfide sheets on Au(111). *J Phys Chem Lett* (2020) 11(21):9038–44. doi:10.1021/acs.jpclett.0c02268

47. Gandubert AD, Krebs E, Legens C, Costa D, Guillaume D, Raybaud P. Optimal promoter edge decoration of CoMoS catalysts: A combined theoretical and experimental study. *Catal Today* (2008) 130(1):149–59. doi:10.1016/j.cattod.2007.06.041

48. Lauritsen JV, Kibsgaard J, Olesen GH, Moses PG, Hinnemann B, Helveg S, et al. Location and coordination of promoter atoms in Co- and Ni-promoted MoS_2-based hydrotreating catalysts. *J Catal* (2007) 249(2):220–33. doi:10.1016/j.jcat.2007.04.013

49. Lauritsen JV, Bollinger MV, Lægsgaard E, Jacobsen KW, Nørskov JK, Clausen BS, et al. Atomic-scale insight into structure and morphology changes of MoS_2 nanoclusters in hydrotreating catalysts. *J Catal* (2004) 221(2):510–22. doi:10.1016/j.jcat.2003.09.015

50. Kibsgaard J, Morgenstern K, Lægsgaard E, Lauritsen JV, Besenbacher F. Restructuring of cobalt nanoparticles induced by formation and diffusion of monodisperse metal-sulfur complexes. *Phys Rev Lett* (2008) 100(11):116104. doi:10.1103/PhysRevLett.100.116104

51. Kibsgaard J, Lauritsen JV, Lægsgaard E, Clausen BS, Topsøe H, Besenbacher F. Cluster-support interactions and morphology of MoS_2 nanoclusters in a graphite-supported hydrotreating model catalyst. *J Am Chem Soc* (2006) 128(42):13950–8. doi:10.1021/ja0651106

52. Füchtbauer HG, Tuxen AK, Li Z, Topsøe H, Lauritsen JV, Besenbacher F. Morphology and atomic-scale structure of MoS_2 nanoclusters synthesized with different sulfiding agents. *Top Catal* (2014) 57(1–4):207–14. doi:10.1007/s11244-013-0176-1

53. van Haandel L, Smolentsev G, van Bokhoven JA, Hensen EJM, Weber T. Evidence of octahedral Co–Mo–S sites in hydrodesulfurization catalysts as determined by resonant inelastic X-ray scattering and X-ray absorption spectroscopy. *ACS Catal* (2020) 10(19):10978–88. doi:10.1021/acscatal.0c03062

54. Yue C, Zhou Y, Liu Y, Feng C, Bao W, Sun F, et al. Achieving ultra-dispersed 1T-Co-MoS_2@HMCS via space-confined engineering for highly efficient hydrogen evolution in the universal PH range. *Inorg Chem Front* (2022) 9:2617–27. doi:10.1039/d2qi00269h

55. Bravo-Sanchez M, Romero-Galarza A, Ramírez J, Gutiérrez-Alejandre A, Solís-Casados DA. Quantification of the sulfidation extent of Mo in CoMo HDS catalyst through XPS. *Appl Surf Sci* (2019) 493:587–92. doi:10.1016/j.apsusc.2019.07.012

56. Kappera R, Voiry D, Yalcin SE, Branch B, Gupta G, Mohite AD, et al. Phase-engineered low-resistance contacts for ultrathin MoS_2 transistors. *Nat Mater* (2014) 13(12):1128–34. doi:10.1038/nmat4080

57. Yao Y, Ao K, Lv P, Wei Q. MoS2 coexisting in 1T and 2H phases synthesized by common hydrothermal method for hydrogen evolution reaction. *Nanomaterials* (2019) 9(6):844. doi:10.3390/nano9060844